Journal of Nuclear Materials 381 (2008) 158–164

Contents lists available at ScienceDirect

Journal of Nuclear Materials

journal homepage: www.elsevier.com/locate/jnucmat

Characterization of heterogeneity and nonlinearity in material properties of nuclear graphite using an inverse method

Lianshan Lin [a], Haiyan Li [a], Alex S.L. Fok [a,*], Mark Joyce [b], James Marrow [b]

[a] School of Mechanical, Aerospace and Civil Engineering, The University of Manchester, P.O. Box 88, Sackville Street, Manchester M60 1QD, UK
[b] School of Materials, The University of Manchester, Grosvenor Street, Manchester M1 7HS, UK

ARTICLE INFO

PACS:
81.05.Uw
81.40.Jj
81.70.Bt
81.70.Fy

ABSTRACT

A finite-element-based inverse method has been developed to allow the characterization of the heterogeneity and nonlinearity in material properties of isotropic nuclear graphite using a single experimental test. The method is implemented into the commercial finite element code ABAQUS using its User Material (UMAT) Subroutine for ease of application. The program has been verified using simulated examples with idealized distributions of elastic modulus and the results showed rapid convergence with good accuracy. Finally, the method was applied to actual mechanical testing of nuclear graphite for which the heterogeneous distribution and nonlinearity of material properties were evaluated.

1. Introduction

The prediction of a component's responses under loading using known material parameters forms the bulk of conventional engineering problems, which can also be called direct problems. Inverse problems, on the other hand, involve the determination of the unknown material parameters of a component using its measured responses to loadings, with both the material parameters and loadings being nontrivial. The responses could be displacements, strains, frequencies of vibration, or temperature etc., depending on the material parameters under consideration. Inverse analysis is especially useful for determining material properties that are highly nonlinear, heterogeneous and anisotropic. In general, methods for solving inverse problems require a solution of the responses in terms of the material parameters. Analytical solutions are only available for structures with relatively simple geometry and loading conditions. As a result, numerical methods, such as the finite element method, are usually employed to allow structures with arbitrary shapes and arbitrary loading conditions to be analyzed. For example, Grédiac et al. [1] employed a virtual-field method to determine the material parameters of thin anisotropic plates in bending; while Moussu and Niviot [2] used the method of superposition to determine the elastic constants of an orthotropic material by studying the free vibrations of a rectangular plate.

Recent developments in speckle interferometry and digital image correlation technique [3], especially in Electronic Speckle Pattern Interferometry (ESPI), have made inverse methods even more powerful as a material characterization technique. In ESPI, the tested object is illuminated by laser light and the speckle pattern is recorded by a CCD camera. The interference of successive speckle patterns created by the laser and observed by the CCD camera includes information of the deformation in each visible point of the measured object with a potential resolution of 10 nm or 1 μm/m. With additional information from interference of reflected light, a full-field displacement map can therefore be obtained by this non-contact method, which provides a tremendous amount of information for performing inverse analysis, allowing complex material properties to be determined using a single experiment. For example, Grédiac et al. [4] calculated the in-plane elastic properties of orthotropic composite plates using the non-uniform strain fields induced in T-shape specimens; while Wang et al. [5] determined the elastic constants for a circular isotropic disc under diametral compression using the displacement map provided by Moire interferometry. A hybrid procedure was presented by Genovese et al. [6] which combined speckle interferometry and numerical optimization to characterize homogeneous orthotropic materials (an eight-ply composite laminate).

In this paper, an iterative inverse approach is presented for the characterization of the heterogeneity and nonlinearity exhibited in the material properties of isotropic nuclear graphite. A mixed numerical-experimental procedure, similar to that of Genovese et al. [6], is adopted, with the in-plane strain fields being obtained from optical methods such as ESPI. Changes in the local Young's modulus were evaluated throughout the whole loading history up to the point of fracture, from which the local strain–stress

* Corresponding author. Present address: Minnesota Dental Research Center for Biomaterials and Biomechanics, 16-212 Moos Tower, 515 Delaware Street, SE, Minneapolis, MN 55455, USA. Tel.: +44 161 275 4327; fax: +44 161 275 4328.
E-mail address: alex.fok@manchester.ac.uk (A.S.L. Fok).

0022-3115/$ - see front matter © 2008 Published by Elsevier B.V.
doi:10.1016/j.jnucmat.2008.07.042

curves were constructed. The method has been implemented into the commercial finite element code ABAQUS [7] for ease of application and has been verified using simple examples.

2. Methods

If the displacement fields (u,v) on the surface of the component under load have been measured, using experiments such as ESPI or Moiré interferometry, the corresponding strain fields can be determined by differentiating the displacements with respect to the spatial coordinates (x,y):

$$\begin{cases} \varepsilon_x = \frac{\partial u}{\partial x}, \\ \varepsilon_y = \frac{\partial v}{\partial y}, \\ \varepsilon_{xy} = \frac{1}{2}\left(\frac{\partial u}{\partial y} + \frac{\partial v}{\partial x}\right). \end{cases} \quad (1)$$

To determine the material parameters using the inverse approach, the experiment is simulated using the finite element method. Approximate or guessed values of the material properties have to be used for the initial analysis. These will inevitably produce strain fields that are different from those obtained experimentally. The approach taken here is to adjust the material parameters iteratively until the numerically predicted strain fields converge towards the target values.

The amount of adjustment in the parameters depends on the difference between the two strain fields. For isotropic materials obeying Hooke's Law, for instance,

$$\Delta E^* = \frac{\varepsilon^* - \varepsilon}{\varepsilon} E^*, \quad (2)$$

where $*$ denotes approximate values predicted by the finite element model. According to (2), if the difference in strains is positive, i.e. the strain has been over-estimated, the stiffness of the material will need to be increased. Conversely, if the difference in strains is negative, the material stiffness will need to be reduced. For heterogeneous materials, this adjustment will be performed for each element individually. It has been found important to take into account the contributions from all strain components. Therefore, for a two-dimensional problem, the following equivalent strain is used in Eq. (2):

$$\varepsilon = \sqrt{\varepsilon_x^2 + \varepsilon_y^2 + \varepsilon_{xy}^2}. \quad (3)$$

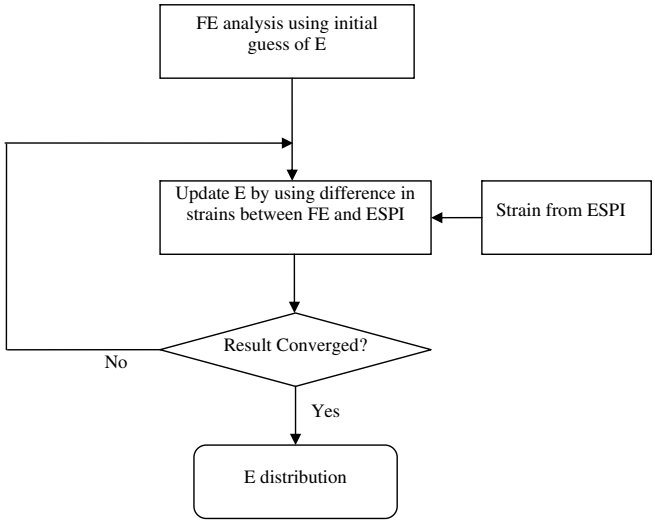

Fig. 1. Flow chart of UMIP (**UM**AT for **I**nverse **P**roblems).

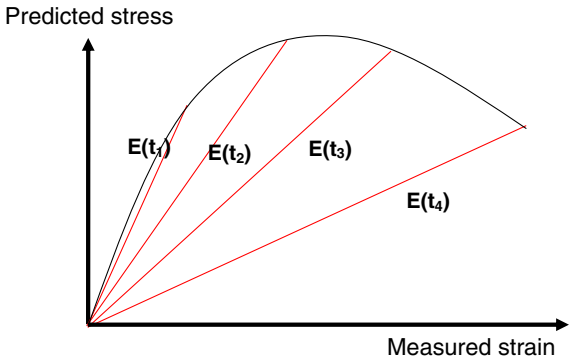

Fig. 2. Construction of nonlinear stress–strain curve using predicted stresses and measured strains. $E(t_i)$ is the Young's modulus determined for load step t_i.

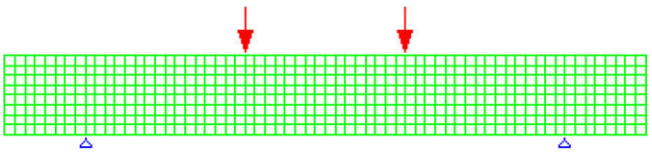

Fig. 3. Finite element model of beam in four-point bending for verification of UMIP.

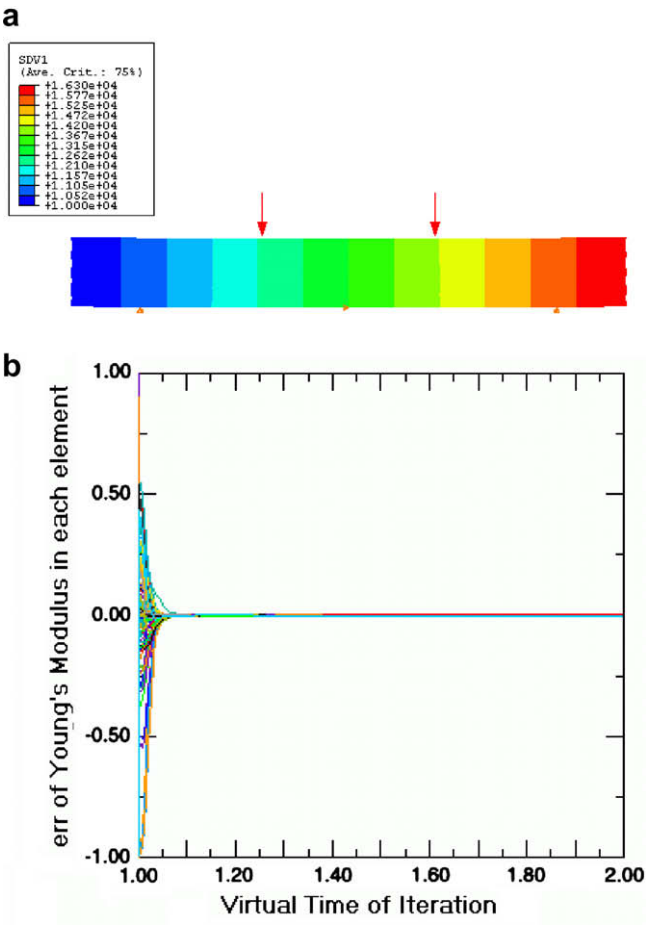

Fig. 4. Verification of UMIP using linearly distributed Young's modulus. (a) Target distribution of E. (b) Error in E predicted by UMIP against iteration time.

The initial guess of Young's Modulus (E_0) can be of any positive value and assumed to be uniform throughout the component. To speed up convergence, it has been found useful to obtain in the

next step a better guess of Young's modulus by assuming that the numerically predicted equivalent stress (σ^*) is similar to the experimental value (σ). Thus,

$$\begin{aligned}&\sigma^* \approx \sigma,\\ &E_1^*\varepsilon_1^* \approx E_1^*\varepsilon = E_0^*\varepsilon_0^*,\\ &E_1^* = E_0^*\varepsilon_0^*/\varepsilon.\end{aligned} \tag{4}$$

Here, the subscript signifies the number of the iteration step. In the subsequent iterations, the adjustment in Young's modulus, ΔE^*, required is

$$\Delta E_i^* = \frac{\varepsilon_i^* - \varepsilon}{(\varepsilon_i^* + \varepsilon)/2} E_{i-1}^*, \quad i = 2, 3, 4, \ldots \tag{5}$$

The use of an average strain in the denominator on the RHS of (3) is to avoid numerical instability in the case of the experimental strain approaching zero. This process is repeated for every element until the numerical values satisfy the convergence criterion.

From past experience, the predicted stresses in non-constrained geometries are not very sensitive to the choice of Poisson's ratio for typical engineering materials, i.e. $\nu \approx 0.2$. For simplicity, therefore, Poisson's ratio was assumed to be constant and uniform, and only the distribution of the Young's modulus E has been determined.

Fig. 1 shows a flow chart of the numerical procedures described above. These have been implemented into ABAQUS [7] using its User Material (UMAT) Subroutine. The particular subroutine has been given the name UMIP which stands for **UM**AT for **I**nverse **P**roblems.

To establish the stress–strain behaviour, which could be nonlinear, strain maps from various load steps throughout the loading history will need to be obtained. The stresses predicted using the Young's modulus determined by the inverse method for each load step can then be used in conjunction with the measured strains to construct the local stress–strain curves. Fig. 2 shows schematically the process involved.

3. Verification tests

Before applying it to actual material characterization, the accuracy and convergence of UMIP needed to be verified. To do so, simple simulations were carried out using a beam in four-point bending as the test configuration. The 'experimental' strain fields were produced using a finite element model (Fig. 3) with the target material property distributions. Two different target E spatial distributions were employed: linear variation along the longitudinal axis and random distribution; see Figs. 4(a) and 5(a). For the latter case, 100 elements out of a total of 512 were given randomly distributed values of E based on the normal distribution:

$$f(x) = \frac{1}{\sqrt{2\pi}\sigma} e^{-\frac{(x-\mu)^2}{2\sigma^2}}, \tag{6}$$

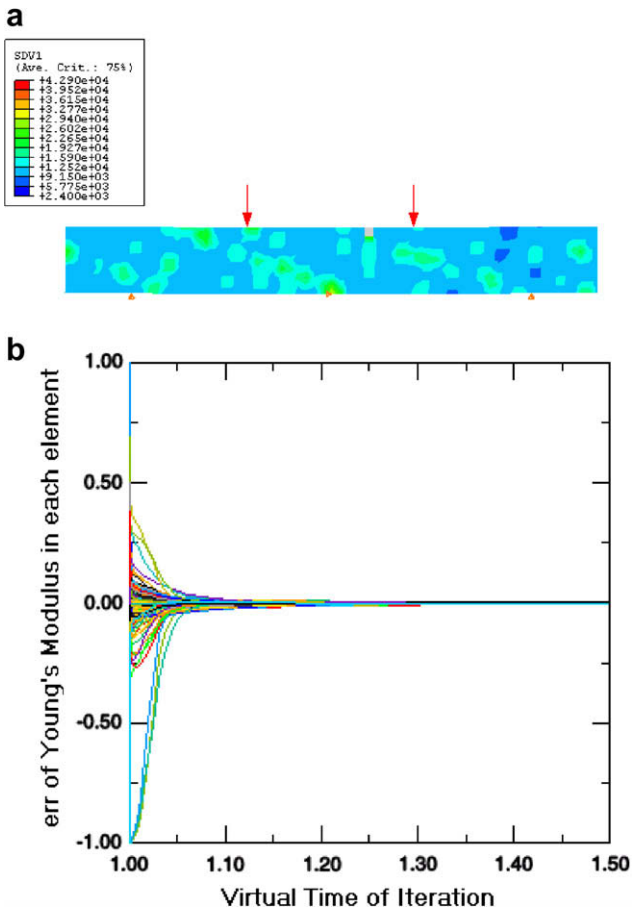

Fig. 5. Verification of UMIP using randomly distributed Young's modulus. (a) Target distribution of E. (b) Error in E predicted by UMIP against iteration time.

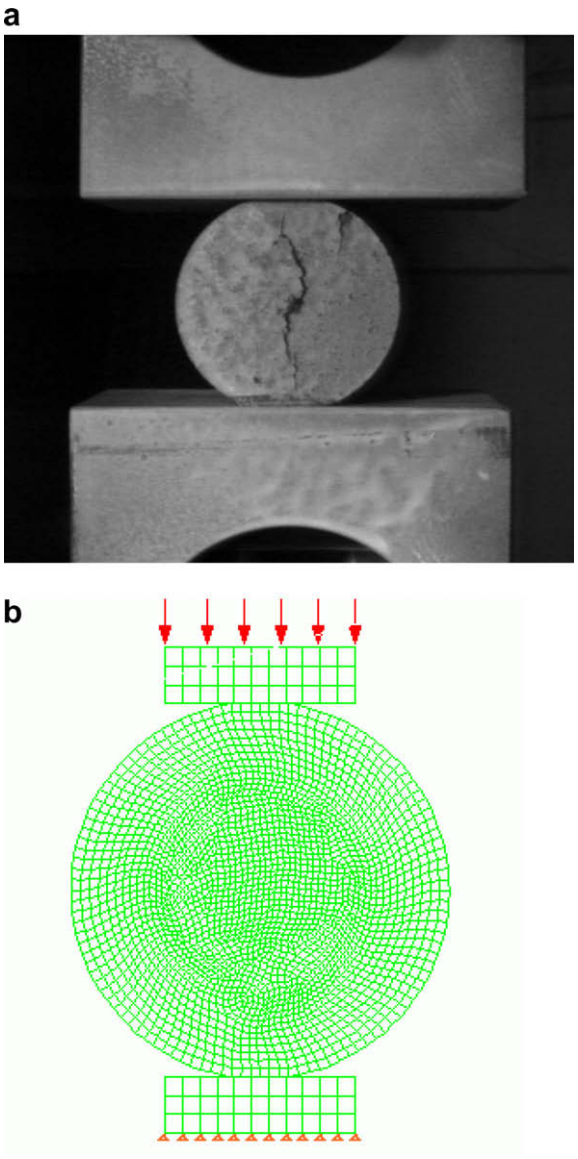

Fig. 6. Nuclear graphite disc under diametral compression. (a) Cracked disc specimen. (b) Finite element model of disc in diametral compression.

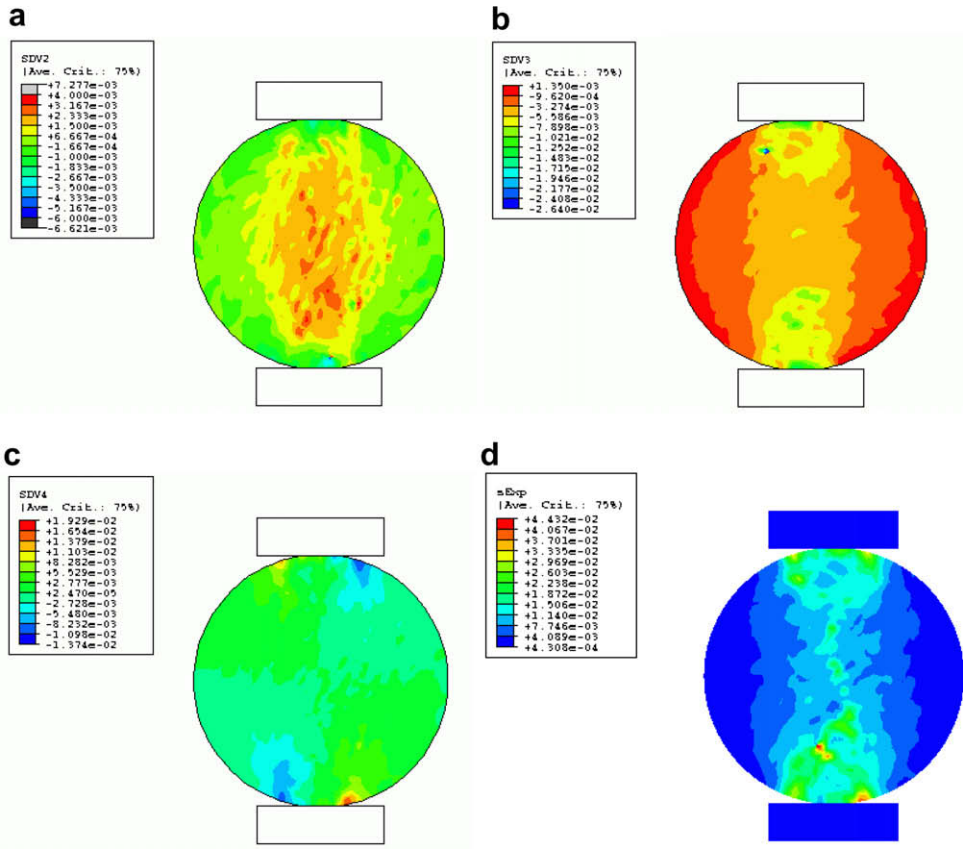

Fig. 7. Experimental strains measured by ESPI at 67% of failure load. (a) Strain X. (b) Strain Y. (c) Strain XY. (d) Equivalent strain.

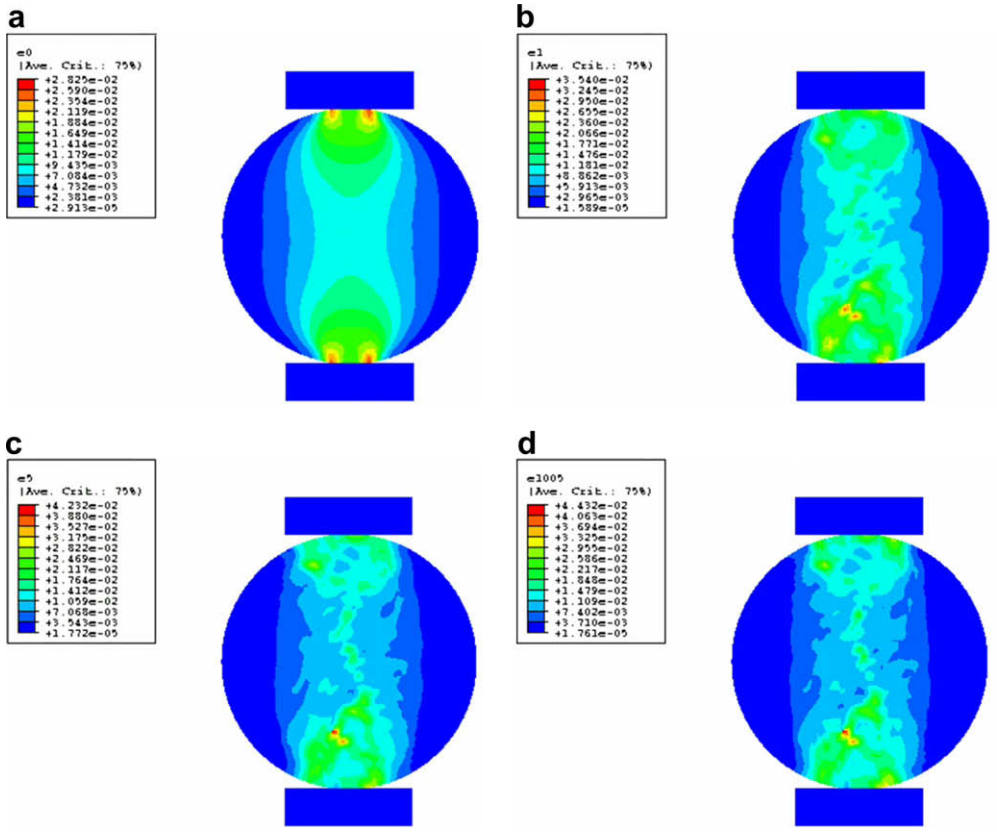

Fig. 8. Evolution of equivalent strain distribution predicted by UMIP at 3.96 kN. Compare the converged result with Fig. 7(d). (a) Time step = 0 (uniform *E* distribution). (b) Time step = 1. (c) Time step = 5. (d) Time step = 1005 (converged result).

where $\mu = 200$, $\sigma = 80$ and $E = x/10$ GPa. The positions of these 100 elements were also randomly selected. The remaining 412 elements were given a Young's modulus of 10 GPa. For both cases, Poisson's ratio was set as a constant of 0.2.

Using the same FE model but different material properties as initial guesses, UMIP was then used to characterize the property distributions based on the simulated 'experimental' strain fields. Figs. 4(b) and 5(b) show the speed of convergence of the results in the form of fractional error in the predicted E for all elements against the number of time steps. It can be seen that, for isotropic but heterogeneous materials, UMIP can give very accurate results which converge quickly.

4. Characterization of material properties of nuclear graphite

The microstructure of isotropic nuclear graphite is a random mixture of filler particles, binder and porosities. These give rise to a random spatial distribution in local elastic properties which will produce a heterogeneous strain field even under uniform loading. Cracks and large pores may act as low stiffness regions, for example. A detailed knowledge of the spatial variation of the local Young's modulus may therefore help to identify possible fracture initiation sites, and provide insight into specimen size dependent properties, such as strength, which may have a Weibull distribution, for example [8,9]. In addition, the onset of significant nonlinear stress–strain behaviour may also indicate the initiation and propagation of microcracking prior to final rupture.

Fracture tests were carried out using isotropic nuclear graphite (IM-124) discs subjected to diametral compression (Fig. 6). Such tests have been used to assess irradiation-induced changes in the strength of graphite samples trepanned from nuclear reactor cores [10]. This loading configuration produces a horizontal tensile stress along the loaded diameter which is roughly a third of the vertical compressive stress. The diameter of the disc used in this work was 20 mm and its thickness 12 mm. Fig. 6 shows a cracked disc specimen and the finite element model used to perform the inverse analysis. The experimental displacement maps at different stages of loading were obtained using ESPI up to the point of fracture. Numerical differentiation of the displacements was then carried out to derive the strains. An example of the strain maps obtained is shown in Fig. 7 for a load of 3.96 kN, i.e. ~67% of the failure load. The vertical, horizontal and shear strains are shown in Fig 7(a)–(c). The derived equivalent strain map is given in Fig. 7(d).

UMIP was used to determine the Young's modulus distribution of the graphite disc, with Poisson's ratio being assumed to be a constant of 0.16 [11]. Fig. 8 shows the evolution of the predicted equivalent strain map for the same data as that of Fig. 7. As can be seen, the converged result is very similar to that shown in Fig. 7(d). Fig. 9 gives the underlying Young's modulus spatial distribution predicted by UMIP. It seems to indicate that the evaluated Young's modulus of graphite is strain-dependent, with the elements experiencing the highest stresses in the central part of the disc having the highest modulus values. However, the figure also indicates that the Young's modulus in the area around the periphery of the disc has been considerably underestimated. This is because the low-strain values in this region of the disc cannot be determined accurately due to noise present in the displacement measurements. Edge effects associated with numerical differentiation might also have introduced additional errors. Given that the solution requires force equilibrium, the Young's modulus in the central region is over-estimated by the analysis in compensation for the lower Young's modulus evaluated in the disc periphery.

Fig. 10 shows the frequency (number of elements) plots of the distribution of Young's modulus in the graphite disc specimen under three different load levels. At the lowest load level (0.22 kN), the results were not reliable due to large inaccuracies in the strain measurements (low displacements relative to the noise). As a result, the Young's modulus values were much underestimated. As loading increases (>3.95 kN), the frequency plot settled to a stable shape. The average Young's modulus for moderate loads (between 1.5 and 4.5 kN) was calculated to be about 6.4 GPa, which is within

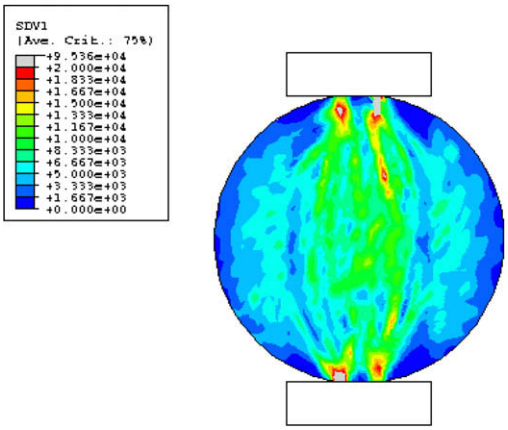

Fig. 9. Young's modulus distribution predicted by UMIP at 3.96 kN.

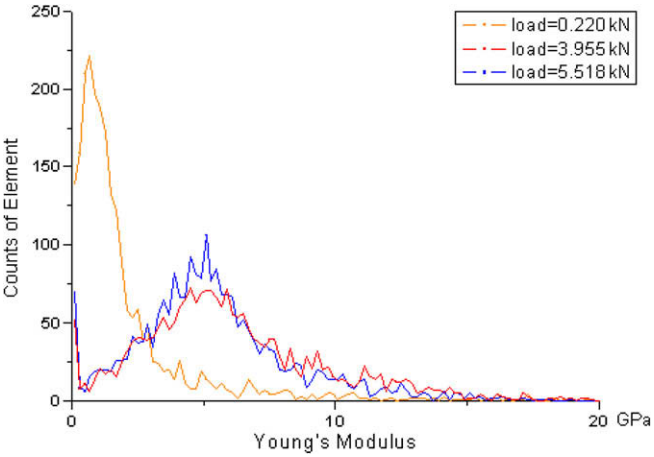

Fig. 10. Frequency distributions of Young's Modulus for graphite disc specimen under different loads.

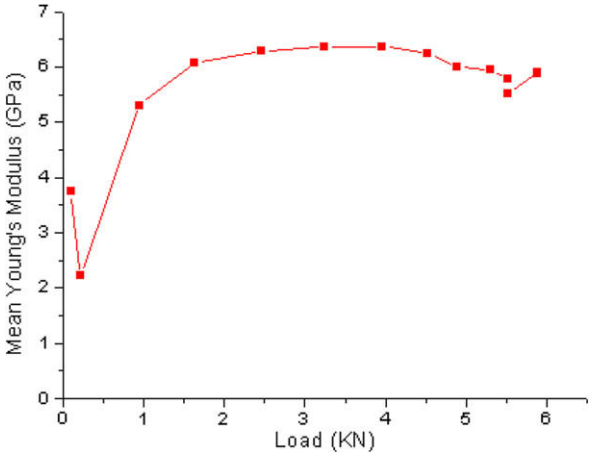

Fig. 11. Mean Young's modulus vs loads.

the scatter band of Young's modulus results determined by assuming homogeneous property and using a least-square fit procedure [12]. Furthermore, this value is consistent with the measured modulus of isotropic graphite under similar levels of compressive stress [11].

Fig. 11 shows the changes in the calculated mean Young's modulus with increasing load. A small drop in the mean modulus value can be observed at the highest load, which is associated with the formation of large macroscopic cracks; see Fig. 6(a).

Fig. 12 further shows the stress–strain behaviours throughout the loading history of selected elements (element 1728, element 1883 and element 2141) close to the disc center where the main crack developed. The positions of these elements are shown in Fig. 12(a). Both the calculated horizontal (tensile) and vertical (compressive) stress components are plotted against their respective measured strains. Figs. 12(c) and(d) show that elements 1883 and 2141 have experienced some form of damage at high stress, as indicated by the change in stiffness gradient with increasing strain in both tensile and compressive directions. This is perhaps not surprising given that both elements lie on the path of the main crack at final fracture. On the other hand, Fig. 12(b) shows that element 1728, which does not lie on the main crack, has retained its stiffness up to the point of failure. The relaxation of compressive strain (and stress) in the compressive vertical direction for this particular element was presumably caused by the removal of load paths due to formation of the main crack nearby.

5. Discussion

The fast convergence and high solution accuracy shown by UMIP in the verification tests indicate that the program is probably robust for the analysis of heterogeneous isotropic materials. However, as for all numerical calculations, the accuracy of the solutions depends largely on the quality of the input data. This was evident in the graphite disc analysis where the displacement measurements contained experimental errors, which have a significant effect on small calculated strains. The effect is seen for Young's modulus, which was underestimated at low load levels when the

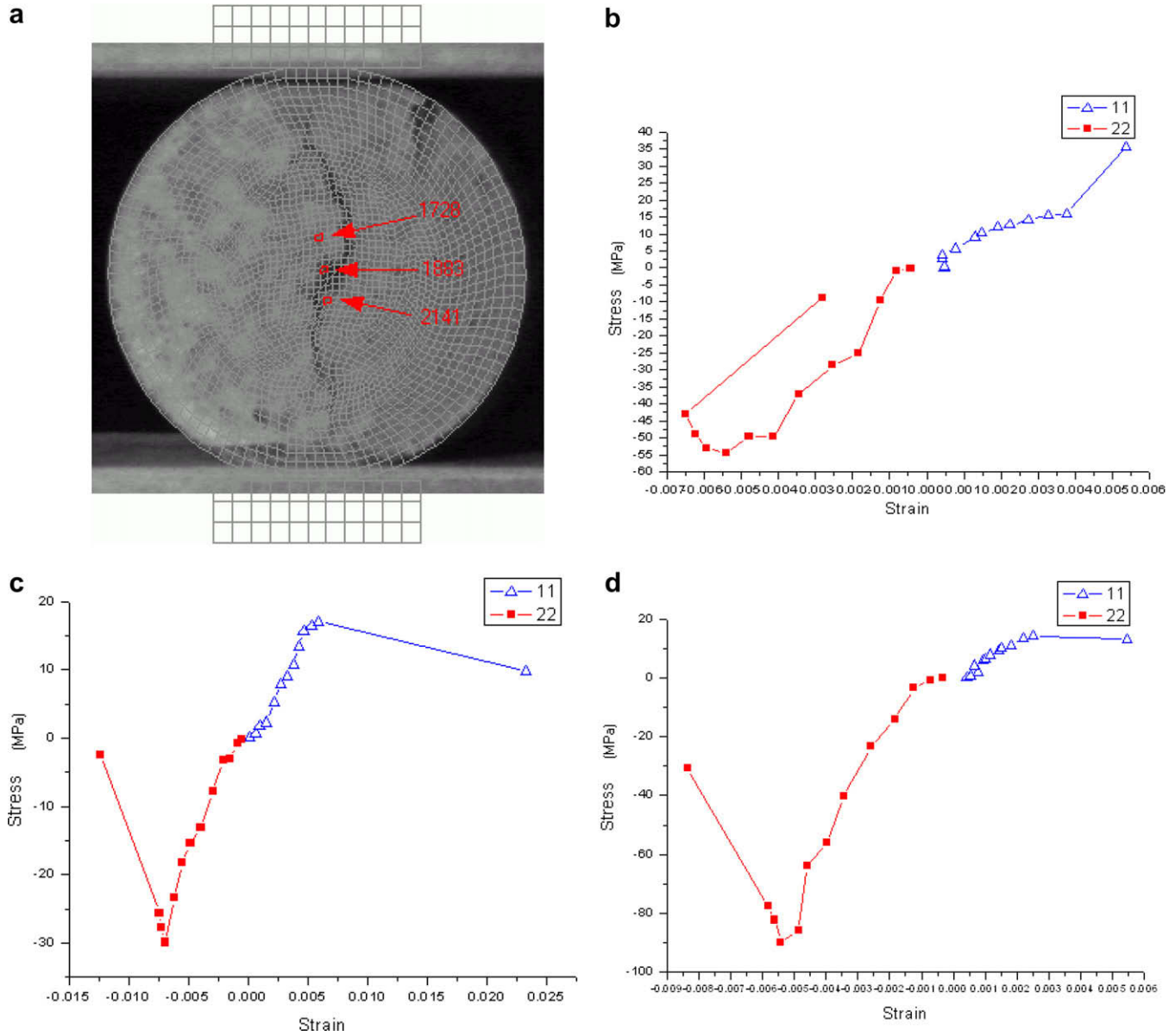

Fig. 12. Strain–stress curves of selected elements. (a) Elements selected for sampling stress–strain behaviour. The cracked disc sample is in the background. (b) Strain–stress curves of element 1728 (11: horizontal direction, 22: vertical direction). (c) Strain–stress curves of element 1883. (d) Strain–stress curves of element 2141.

ratio of noise to true response was high. The same happened to low-strain regions, mainly in the periphery of the disc, even at moderate to high load levels. This probably caused an overestimation of Young's modulus in the central region in order to compensate and maintain equilibrium. The observed increase in modulus with stress is therefore an artifact of the analysis, and not necessarily the true material behaviour. Nevertheless, the program appeared to be capable of predicting reasonably well the overall stress–strain behaviour exhibited by graphite materials up to the point of fracture. Better results are expected with reduction of noise in the measured displacement maps. This can be achieved by optimization of the optics and mechanical stability of the measurements, and this work is in progress.

The application of UMIP to the analysis of the bridging and damage process zones around a crack tip is likely to produce rewarding results. With the ability to quantify the elastic modulus and hence the strain energy within these regions, one can gain a better, quantitative understanding of the damage mechanism taking place during crack initiation and propagation. The results will also help to validate continuum failure models developed for graphite [13,14].

The program can of course be applied to other quasi-brittle materials, e.g. concrete and ceramics. Further, it can be extended to analyse anisotropic materials such as C–C or SiC–SiC composites, in which case the different strain components will need to be considered separately. However, convergence will probably be more difficult to achieve as there are likely to be multiple solutions for the same displacement map.

6. Concluding remarks

A finite-element-based inverse method has been developed to determine the distribution of material properties of isotropic but heterogeneous materials using full-field strain maps. The method has been implemented into the commercial finite element code ABAQUS through its User Material (UMAT) Subroutine. Verification of the program (UMIP) using simple examples has shown rapid convergence and high accuracy in the predicted Young's modulus distribution. Application of the program to nuclear graphite discs under diametral compression has predicted Young's modulus close to the expected value. In addition, local stress–strain behaviour can be obtained from which the damage evolution of the material together with its spatial variation can be characterized.

Acknowledgements

The financial support of Nexia Solutions is gratefully acknowledged. The graphite material was kindly supplied by British Energy Generation Ltd. The views expressed in this paper are those of the authors and do not necessarily represent the views of the sponsor.

References

[1] M. Grédiac, E. Toussaint, F. Pierron, Int. J. Solids Struct. 40 (2003) 2401.
[2] F. Moussu, M. Niviot, J. Sound Vib. 165 (1) (1993) 149.
[3] D. Amodio, G.B. Broggiato, F. Campana, G.M. Newaz, Exp. Mech. 43 (4) (2003) 396.
[4] M. Grédiac, F. Pierron, Y. Surrel, Exp. Mech. 39 (2) (1998) 42.
[5] Z. Wang, J.F. Cárdenas-García, B. Han, Exp. Mech. 45 (1) (2005) 27.
[6] K. Genovese, L. Lamberti, C. Pappalettere, Exp. Mech. 44 (6) (2004) 584.
[7] HKS, ABAQUS/Analysis User's Manual, Version 6.4-1, 2003.
[8] C.R. Kennedy, Carbon 31 (3) (1993) 519.
[9] B.C. Mitchell, J. Smart, S.L. Fok, B.J. Marsden, J. Nucl. Mater. 322 (2003) 126.
[10] L. Whitworth, Nucl. Eng. 45 (4) (2004) 15.
[11] R. Taylor, R.G. Brown, K. Gilchrist, E. Hall, A.T. Hodds, B.T. Kelly, F. Morris, Carbon 5 (1967) 518.
[12] M.R. Joyce, T.J. Marrow, in: Ageing Management of Graphite Reactor Cores, Cardiff, UK, November 2005.
[13] Z. Zou, S.L. Fok, S.O. Oyadiji, B.J. Marsden, J. Nucl. Mater. 324 (2004) 116.
[14] Z. Zou, S.L. Fok, B.J. Marsden, S.O. Oyadiji, Eng. Fract. Mech. 73 (3) (2006) 318.